

# Estimating the limit of decadal-scale climate predictability using observational data

Ruiqiang Ding<sup>1</sup> · Jianping Li<sup>2,3</sup> · Fei Zheng<sup>4</sup> · Jie Feng<sup>1</sup> · Deqiang Liu<sup>1</sup>

Received: 7 October 2014 / Accepted: 16 May 2015 / Published online: 29 May 2015  
© Springer-Verlag Berlin Heidelberg 2015

**Abstract** Current coupled atmosphere–ocean general circulation models can not simulate decadal variability well, and model errors would have a significant impact on the estimation of decadal predictability. In this study, the nonlinear local Lyapunov exponent method is adopted to estimate the limit of decadal predictability based on 9-year low-pass filtered sea surface temperature (SST) and sea level pressure (SLP) observations. The results show that the limit of decadal predictability of the SST field is relatively large in the North Atlantic, North Pacific, Southern Ocean, tropical Indian Ocean, and western North Pacific, exceeding 7 years at most locations in these regions. In contrast, the limit of the SST field is relatively small in the tropical central–eastern Pacific (4–6 years). Similar to the SST field, the SLP field has a relatively large limit of decadal predictability over the Antarctic, North Pacific, and tropical Indian Ocean (>6 years). In addition, a relatively large limit of decadal predictability of the SLP field also occurs over the land regions of Africa, India, and South America. Distributions of the limit of decadal predictability of both the SST and SLP fields are almost consistent with those of their intensity and persistence on decadal

timescales. By examining the limit of decadal predictability of several major climate modes, we found that the limit of decadal predictability of the Pacific decadal oscillation (PDO) is about 9 years, slightly lower than that of the Atlantic multi-decadal oscillation (AMO) (about 11 years). In contrast, the northern and southern annular modes have limits of decadal predictability of about 4 and 9 years, respectively. However, the above limits estimated using time-filtered data may overestimate the predictability of decadal variability due to the use of time filtering. Filtered noise with the same spectral characteristics as the PDO and AMO, has a predictability of about 3 years. Future work is required with a longer period of observations or using a more realistic model of decadal variability to assess the real-time decadal predictability.

**Keywords** Decadal-scale climate predictability · Nonlinear local Lyapunov exponent (NLLE) · Initial-value decadal predictability limit

## 1 Introduction

The use of dynamical and statistical models for seasonal forecasting has becoming widespread over the past two decades, and now many operational and research centers routinely make seasonal forecasts. The success of seasonal forecasting is, to a large extent, due to the increased understanding of the sources and limits of seasonal predictability. It has long been recognized that most of the current seasonal predictive skill over many regions of the world comes from the strong influence of the El Niño–Southern oscillation (ENSO) phenomenon (e.g., Shukla 1984; Goswami and Shukla 1991; Lau and Nath 1996; Chang et al. 2003; Wang et al. 2009; Kumar et al. 2013), which can be predicted with a lead time of up to 1 year (Latif et al. 1998;

✉ Jianping Li  
ljp@lasg.iap.ac.cn; ljp@bnu.edu.cn

<sup>1</sup> State Key Laboratory of Numerical Modeling for Atmospheric Sciences and Geophysical Fluid Dynamics (LASG), Institute of Atmospheric Physics, Chinese Academy of Sciences, Beijing 100029, China  
<sup>2</sup> College of Global Change and Earth System Sciences (GCESS), Beijing Normal University, Beijing 100875, China  
<sup>3</sup> Joint Center for Global Change Studies, Beijing 100875, China  
<sup>4</sup> International Center for Climate and Environmental Sciences (ICCES), Institute of Atmospheric Physics, Chinese Academy of Sciences, Beijing 100029, China

Collins et al. 2002; Zheng et al. 2006; Jin et al. 2008; Li and Ding 2013).

In recent years, climate predictions over interannual to decadal timescales have received increased attention (e.g., Latif et al. 2004; Keenlyside et al. 2008; Meehl et al. 2009; Pohlmann et al. 2009; Mehta et al. 2011; Lienert and Doblas-Reyes 2013). These predictions fill the gap between seasonal and climate change predictions, and can provide useful information on the climate conditions and risks that we might experience over coming decades, which is extremely valuable for decision-making in various sectors such as agriculture, energy, and infrastructure development. However, in contrast to seasonal forecasting, interannual to decadal climate prediction is at an early stage of development (Murphy et al. 2010). To date, little is known of the sources and limits of decadal predictability at regional and global scales. In the context of current efforts to improve decadal climate predictions, there is a need to examine these sources and limits of decadal-scale predictability. In the present study, we focus our efforts on the limits of decadal-scale climate predictability within the global atmosphere–ocean system.

Many previous studies have examined decadal-scale predictability (e.g., Griffies and Bryan 1997; Boer 2000, 2004, 2011; Collins 2002; Collins and Sinha 2003; Pohlmann et al. 2004), and they used two common approaches: the diagnostic approach and the prognostic approach. In the diagnostic approach, the variance of a climate variable is decomposed into a potentially predictable signal component and an unpredictable noise component. Potential decadal predictability is analyzed using the ratio of the signal variance to the noise variance. In the prognostic approach, the decadal predictability is estimated from perfect model experiments, which use a coupled atmosphere–ocean general circulation model (CGCM). The perfect model ensemble experiments use identical oceanic and perturbed atmospheric initial conditions and are performed to quantify the spread within the ensemble relative to the variability of the control run, which may then be used to make an estimate of predictability. This approach gives an upper limit of predictability as it assumes a perfect model and identical oceanic initial conditions. Both the diagnostic and prognostic approaches have indicated that some useful decadal predictability may exist in four regions: the North Atlantic, Southern Ocean, North Pacific, and tropical Pacific (Latif et al. 2006). The North Atlantic and Southern Ocean have been found to be the two most predictable regions. These two regions are predictable over periods of up to 10 years or longer (Boer 2000; Collins and Sinha 2003; Pohlmann et al. 2004).

These studies have significantly improved our understanding of decadal predictability. However, as pointed out by Latif et al. (2006), there has been a heavy reliance

on models in decadal predictability estimates. While models have been helpful in identifying possible mechanisms, almost all CGCMs in use today, such as the Intergovernmental Panel on Climate Change (IPCC) Fifth Assessment Report (AR5) coupled models (Flato et al. 2013), are imperfect, and uncertainties remain with respect to the simulation of decadal variability. Any such model errors will have a significant influence on estimates of decadal predictability; consequently, these estimates may not reflect the true predictability of decadal variability. Given the lack of realistic CGCMs currently available for simulating decadal variability, it is appropriate to investigate decadal predictability based on observational data.

Recently, a new method based on the nonlinear local Lyapunov exponent (NLLE) was introduced to investigate atmospheric and oceanic predictability using observational data (Chen et al. 2006; Ding and Li 2007; Li and Wang 2008; Li and Ding 2011). The NLLE method, which is a nonlinear extension of the traditional Lyapunov exponent concept, can quantitatively determine the limit of atmospheric and oceanic predictability over various timescales by exploring the evolution of the distance between initially local dynamical analogs (LDAs) from the observational time series. Accordingly, the predictability of decadal climate variability can be assessed by applying the NLLE method to observational data. In this study, on the basis that the limit of decadal predictability of the global atmosphere–ocean system varies widely with region, we investigate the spatial distributions of the limit of decadal predictability of the sea surface temperature (SST) and sea level pressure (SLP) fields using the NLLE method to identify the regions of relatively high decadal predictability.

Furthermore, the Pacific decadal oscillation (PDO; Mantua et al. 1997; Zhang et al. 1997) and Atlantic multidecadal oscillation (AMO; Schlesinger and Ramankutty 1994), which are known as the dominant decadal SST modes in the North Pacific and North Atlantic, respectively, have widespread effects on temperatures and precipitation across North American and Eurasia (Mantua and Hare 2002; Sutton and Hodson 2005; Knight et al. 2006; Zhang et al. 2007). The northern annular mode (NAM, also known as the Arctic oscillation (AO); Thompson and Wallace 1998; Li and Wang 2003) and southern annular mode (SAM, also known as the Antarctic oscillation (AAO); Gong and Wang 1999; Nan and Li 2003) are major climate modes in the SLP field and link mid-latitudes to the polar regions of the Northern and Southern Hemispheres, respectively, exerting a marked impact on climate throughout much of their respective hemispheres (e.g., Deser and Timlin 1997; Hurrell et al. 2001; Marshall et al. 2001; Prieto et al. 2002; Buermann et al. 2005; Codron 2005; Verdy et al. 2005; Liu and Ding 2007; Stammerjohn et al. 2008). The NAM and SAM have also been shown to exhibit decadal variability

and trends (Molinari and Mestas-Nuñez 2003; Ostermeier and Wallace 2003; Yuan and Yonekura 2011). Based on the indices of these climate modes, the NLLE method can also be used to investigate the limit of decadal predictability of these major modes of oceanic and atmospheric variability. We note that the limit of decadal predictability obtained in the present study would be lower than the theoretical upper limit of decadal predictability, which may be achieved only if the prediction model is perfect except for sufficiently small errors in the initial conditions.

The remainder of this paper is organized as follows. Section 2 describes the data used in this study. Section 3 introduces the NLLE method. Section 4 examines the spatial distributions of the limit of decadal predictability of the SST and SLP fields. Section 5 presents the results of the predictability analysis of several major climate modes using the NLLE method. The influences of dataset length and temporal filtering on predictability estimates are discussed in Sect. 6. Finally, Sect. 7 summarizes and discusses the major results.

## 2 Data

The observations used in this study were a range of century-long gridded climate analyses. The monthly gridded SST dataset used was version 3 of the Extended Reconstructed SST (ERSST.v3) generated by the National Oceanic and Atmospheric Administration (NOAA) on a  $2^\circ \times 2^\circ$  spatial grid (Smith et al. 2008), covering the period 1854–2011. The updated version of the monthly Extended Kaplan SST data obtained from the UK Met Office SST data (Reynolds and Smith 1994; Kaplan et al. 1998), with a spatial resolution of  $5^\circ$  and covering the period 1856–2011, was used to verify results from ERSST. Atmospheric data (in particular, SLP data) were obtained from the Hadley Centre (HadSLP) on a  $2^\circ \times 2^\circ$  spatial grid (Allan and Ansell 2006) and cover the period 1850–2011. In addition, we used the reconstructed monthly SLP field from 1659 to 1999 over the eastern North Atlantic and Europe (Luterbacher et al. 2002) to check the dependence of the estimated limit of decadal predictability on the length of the dataset.

The PDO index for the period 1854–2011 is defined as the leading principal component (PC) of monthly SST anomalies in the North Pacific poleward of  $20^\circ\text{N}$  (Mantua et al. 1997; Zhang et al. 1997), and was derived from the ERSST dataset. The AMO index over the same period was calculated by averaging detrended monthly SST anomalies over the extratropical North Atlantic region ( $30^\circ\text{N}$ – $65^\circ\text{N}$ ,  $75^\circ\text{W}$ – $7.5^\circ\text{W}$ ; Trenberth et al. 2007), and was also derived from the ERSST dataset. The monthly SAM index over the period 1850–2011 is defined as the difference in the normalized monthly zonal-mean SLP between  $40^\circ\text{S}$  and  $70^\circ\text{S}$

(Nan and Li 2003), while the monthly NAM index over the same period is defined as the difference in the normalized monthly zonal-mean SLP between  $35^\circ\text{N}$  and  $65^\circ\text{N}$  (Li and Wang 2003). Both the SAM and NAM indices were derived from the HadSLP dataset.

## 3 Introduction to the NLLE method

### 3.1 NLLE of an $n$ -dimensional dynamical system

Consider a general  $n$ -dimensional nonlinear dynamical system whose evolution is governed by

$$\frac{d\mathbf{x}}{dt} = \mathbf{F}(\mathbf{x}), \tag{1}$$

where  $\mathbf{x} = [x_1(t), x_2(t), \dots, x_n(t)]^T$  is the state vector at the time  $t$ , the superscript T is the transpose, and  $\mathbf{F}$  represents the dynamics. The evolution of a small error  $\delta = [\delta_1(t), \delta_2(t), \dots, \delta_n(t)]^T$ , superimposed on a state  $\mathbf{x}$ , is governed by the nonlinear equation:

$$\frac{d}{dt}\delta = \mathbf{J}(\mathbf{x})\delta + \mathbf{G}(\mathbf{x}, \delta), \tag{2}$$

where  $\mathbf{J}(\mathbf{x})\delta$  are the tangent linear terms, and  $\mathbf{G}(\mathbf{x}, \delta)$  are the high-order nonlinear terms of the error  $\delta$ . Due to some difficulties in solving the nonlinear problem, most previous studies (e.g., Lorenz 1965; Eckmann and Ruelle 1985; Yoden and Nomura 1993; Kazantsev 1999; Ziehmman et al. 2000) assumed that the initial perturbations were sufficiently small that their evolution could be approximately governed by the tangent linear model (TLM) of the nonlinear model. However, the tangent linear approximation to error growth equations has many limitations in predictability problems involving finite-amplitude initial errors (Lacarra and Talagrand 1988; Mu 2000; Ding and Li 2007; Li and Ding 2011). Therefore, we should take into account the nonlinear behaviors of error growth when determining the limit of predictability. Without a linear approximation, the solutions of Eq. (2) can be obtained by numerical integration along the reference solution  $\mathbf{x}$  from  $t = t_0$  to  $t_0 + \tau$ :

$$\delta_1 = \boldsymbol{\eta}(\mathbf{x}_0, \delta_0, \tau)\delta_0, \tag{3}$$

where  $\delta_1 = \delta(t_0 + \tau)$ ,  $\mathbf{x}_0 = \mathbf{x}(t_0)$ ,  $\delta_0 = \delta(t_0)$ , and  $\boldsymbol{\eta}(\mathbf{x}_0, \delta_0, \tau)$  is the nonlinear propagator. The NLLE is then defined as

$$\lambda(\mathbf{x}_0, \delta_0, \tau) = \frac{1}{\tau} \ln \frac{\|\delta_1\|}{\|\delta_0\|}, \tag{4}$$

where  $\lambda(\mathbf{x}_0, \delta_0, \tau)$  depends in general on the initial state  $\mathbf{x}_0$  in phase space, the initial error  $\delta_0$ , and time  $\tau$ . The NLLE differs from existing local or finite-time Lyapunov exponents defined based on linear error dynamics (Yoden and

Nomura 1993; Kazantsev 1999; Ziehmann et al. 2000), which depend solely on the initial state  $\mathbf{x}_0$  and time  $\tau$ , and not on the initial error  $\delta_0$ . The ensemble mean NLLE over the global attractor of the dynamical system is given by

$$\begin{aligned} \bar{\lambda}(\delta_0, \tau) &= \int_{\Omega} \lambda(\mathbf{x}_0, \delta_0, \tau) d\Omega \\ &= \langle \lambda(\mathbf{x}_0, \delta_0, \tau) \rangle_N, \quad (N \rightarrow \infty) \end{aligned} \tag{5}$$

where  $\Omega$  represents the domain of the global attractor of the system and  $\langle \cdot \rangle_N$  denotes the ensemble average of samples of sufficiently large size  $N$  ( $N \rightarrow \infty$ ). The ensemble mean NLLE reflects the global evolution of mean error growth over an attractor and can measure global mean predictability. The mean relative growth of the initial error (RGIE) can be obtained by:

$$\bar{\Phi}(\delta_0, \tau) = \exp \left[ \bar{\lambda}(\delta_0, \tau) \tau \right]. \tag{6}$$

For chaotic systems, using the theorem from Ding and Li (2007), we obtain

$$\bar{\Phi}(\delta_0, \tau) \xrightarrow{P} c(N \rightarrow \infty), \tag{7}$$

where  $\xrightarrow{P}$  denotes the convergence in probability and  $c$  is a constant that depends on the converged probability distribution  $P$  of error growth. The constant  $c$  can be considered to be the theoretical saturation level of  $\bar{\Phi}(\delta_0, \tau)$ . According to the dynamical systems theory, the error saturation value represents the average distance between two randomly chosen points over a chaotic attractor, implying that once the error growth reaches the saturation level, almost all information on initial states is lost and the prediction becomes meaningless. Using the theoretical saturation level, the limit of dynamical predictability can be quantitatively determined (Ding and Li 2007; Li and Ding 2011).

### 3.2 Estimating the NLLE from an observational time series

For nonlinear dynamical systems whose equations of motion are explicitly known, such as the Lorenz system (Lorenz 1963), we can directly calculate the mean NLLE via numerical integration of their error evolution equations (Ding and Li 2007). In addition, if large amounts of observational or experimental data are available for dynamical systems, we can estimate the mean NLLE by making use of these data when the evolution equations of the systems are unknown or incomplete. In previous studies, we developed an algorithm that yields estimates of the NLLE and its derivatives based on observational data (Ding et al. 2008; Li and Ding 2011). The general purpose of this algorithm is to find local analogs of the evolution pattern from observational time series. The local analogs are searched for based

on the initial information and evolution information at two different time points in the time series. If the initial distance at two different time points is small, and if their evolutions are analogous over a very short interval, it is very likely that the two points were analogous at the initial time. This analog is referred to as a LDA. The mean NLLE is then estimated by calculating the mean exponential divergence rate of LDAs, and the mean error growth is obtained by calculating the mean RGIE between all LDAs. A brief description of the algorithm is given in ‘‘Appendix 1’’. This NLLE method has been applied to atmospheric and oceanic observational data to investigate decadal changes in weather predictability (Ding et al. 2008), the temporal–spatial distributions of predictability limits of the daily geopotential height and wind fields (Li and Ding 2011), the temporal–spatial distributions of predictability limits of monthly and seasonal means of various climate variables (Li and Ding 2008, 2013), and the predictability limit of the intraseasonal oscillation (ISO) (Ding et al. 2010, 2011).

Figure 1 shows a schematic illustration of the mean error growth for a chaotic system in which the growth of sufficiently small errors is initially exponential with a growth rate consistent with the maximal Lyapunov exponent, as obtained using the NLLE method. We can see that the mean error growth initially increases quickly, then slows down, and finally reaches a saturation value. In contrast, the linear error evolution shows a continuous exponential growth. These results show that the linear error approximation is not suitable for describing the processes from initial exponential growth to saturation for sufficiently small errors. The nonlinear properties of the NLLE make it applicable to describing the processes associated with nonlinear error growth in chaotic systems,

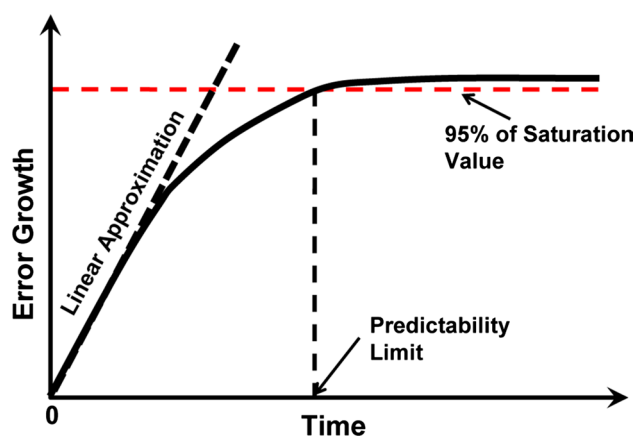


**Fig. 1** Schematic illustration of the determination of the predictability limit from the mean error growth as a function of time, obtained using the NLLE method. The mean error growth on the y-axis uses a logarithmic scale to amplify the differences between linear and nonlinear error evolutions

thereby overcoming the limitations of traditional linear error dynamics. According to the dynamical systems theory, the time at which the error reaches its saturation level is specified as the predictability limit. However, in practice, considering that the saturation level of error growth is not constant, but is subject to small fluctuations (see Figs. 9, 10) when a relatively small number of data points is used to estimate the NLLE, the predictability limit in this study is defined as the time at which the error reaches 95 % of its saturation value, in order to reduce the effect of error fluctuations. The saturation value is obtained by taking the average of the mean error growth after the error almost stops increasing (i.e., the error growth rate close to 0), following the work of Li and Ding (2011). Accordingly, we can quantitatively determine the predictability limit based on the nonlinear error evolution curve, as shown in Fig. 1.

#### 4 Spatial distributions of the limit of decadal predictability

This section focuses on investigating the spatial distributions of the limit of decadal predictability of the SST and SLP fields. To extract the decadal components of the SST and SLP, the climatological mean annual cycle and linear trend were removed from the monthly SST and SLP data at each grid point, leaving the anomalies, which were then passed through a 9-year low-pass Gaussian filter. The subtraction of the linear trend is expected to reduce effects due to global warming. In this way, the annual cycle, interannual, and secular trend components are removed from the monthly data, leaving the (mostly) decadal anomalies. Next, we explored the spatial distributions of the predictability limit of the filtered SST and SLP fields using the NLLE method.

Figure 2a shows the spatial distribution of the predictability limit of the 9-year low-pass filtered SST based on the ERSST dataset. The limit of decadal predictability of the SST ranges from about 4 to 12 years, largely depending on the location. It is relatively high in five main regions: the North Atlantic, North Pacific, Southern Ocean, tropical Indian Ocean, and western North Pacific. The limit of decadal predictability at most locations in these regions exceeds 7 years. In contrast, in the tropical central–eastern Pacific, where the climate signal is dominated by interannual variability associated with ENSO, the predictability limit of the 9-year low-pass filtered SST is relatively low (4–6 years). Overall, the zonal mean limit of decadal predictability of the SST is higher in the extratropics than in the tropics (Fig. 2b), which is exactly the opposite of the zonal mean limit of monthly to interannual SST predictability (Li and Ding 2013).

The spatial distribution of the limit of decadal predictability of SST is consistent with that of the intensity of decadal SST variability (as represented by the ratio of the 9-year low-pass filtered variance to the total variance of the annual mean SST time series, shown as a percentage in Fig. 3a). The regions where decadal SST variability is relatively strong (for example, the North Atlantic, North Pacific, Southern Ocean, tropical Indian Ocean, and western North Pacific) have a relatively high limit of decadal predictability; in contrast, the regions where decadal SST variability is relatively weak (for example, the tropical central–eastern Pacific) have a relatively low limit of decadal predictability. Both distributions have a spatial correlation of 0.67 (significant at the 0.001 level), indicating that the predictability limit of decadal SST variability is closely related to its intensity.

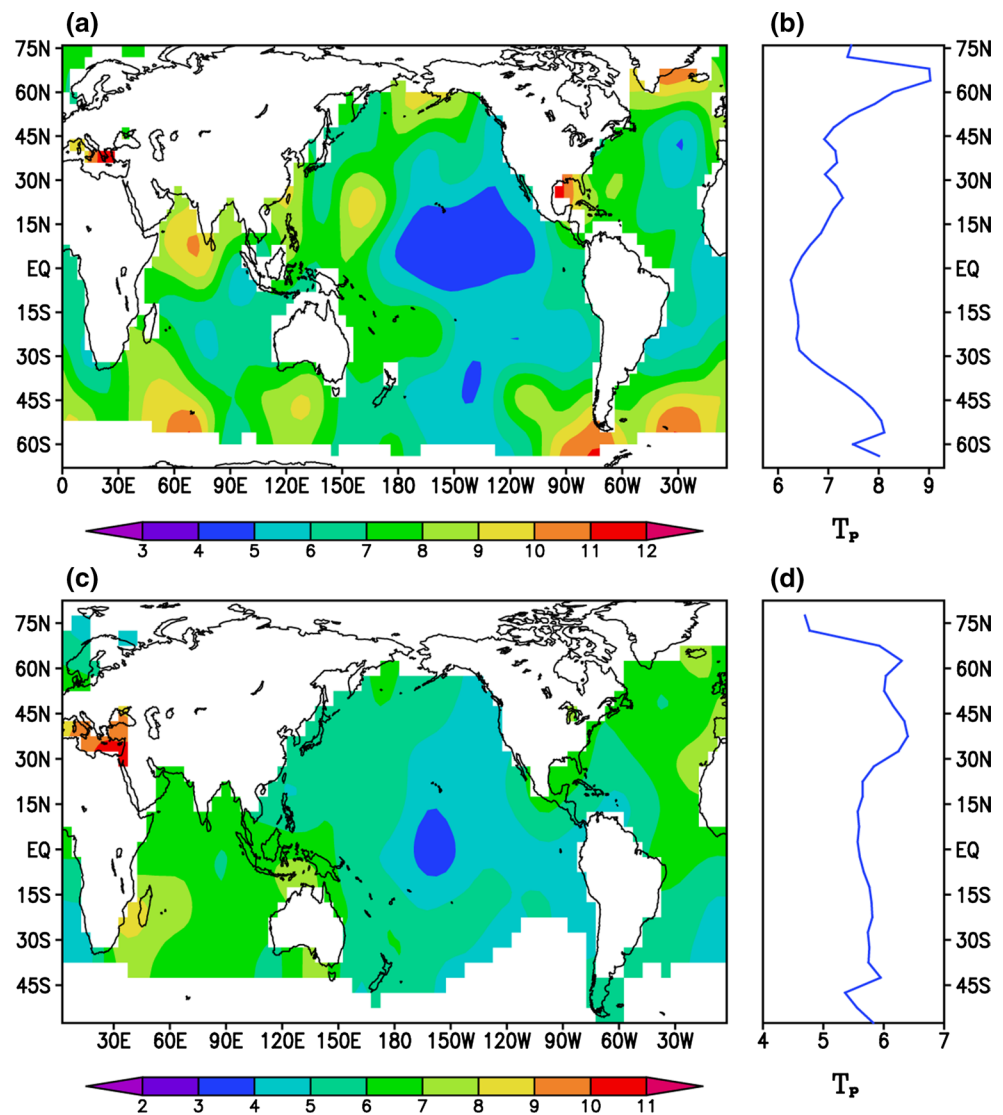
The prominent decadal climate variability in the North Atlantic and North Pacific has been extensively documented in the literature (e.g., Schlesinger and Ramankutty 1994; Mantua et al. 1997; Zhang et al. 1997; Delworth and Mann 2000). In contrast, few studies have examined the decadal variability of the Southern and Indian oceans. However, there is observational evidence of marked decadal and multidecadal variations in the Southern and Indian oceans (Yuan and Yonekura 2011; Nidheesh et al. 2012; O’Kane et al. 2013; Han et al. 2014). In general, our results confirm these previous findings, and additionally suggest that regions with a large decadal variability tend to have a relatively high limit of decadal predictability. A similar phenomenon also occurs over interannual timescales. Kirtman and Schopf (1998) reported that, during decades when the amplitude of the interannual variability of ENSO is large, the forecast skill of ENSO is relatively high and the predictability limit of ENSO is relatively long. Furthermore, Tang et al. (2005) explicitly built a mathematical relationship between ENSO variability and its predictability.

The distribution of the limit of decadal predictability of the Kaplan SST (Fig. 2c) is qualitatively similar to that from ERSST. However, in contrast to ERSST, the Kaplan SST shows relatively lower values of the limit of decadal predictability over most of the global oceans. A possible explanation for this difference may be that the Kaplan SST exhibits a weaker intensity of decadal variability over most of the global oceans compared with the ERSST data (Fig. 3b).

The above analysis indicates that the North Atlantic, Southern Ocean, and North Pacific are three regions of high decadal SST predictability, and this is consistent with the findings of previous studies (Boer 2000, 2004; Pohlmann et al. 2004; Latif et al. 2006). However, the present results indicate that in addition to these three regions, the tropical Indian Ocean and western Pacific (i.e., the Indo-western Pacific) are also regions of high predictability, and



**Fig. 2** **a** Spatial distribution of the predictability limit ( $T_p$ , in years) of the 9-year low-pass filtered SST and **b** its zonal mean profile based on the ERSST dataset. **c, d** As **(a, b)**, respectively, but based on the Kaplan SST dataset



this was not noted by these previous studies. In contrast, Boer (2000) reported that there is a high predictability over the tropical Pacific for the decadal means of surface air temperature (SAT). The different results obtained in the present study and by Boer (2000) may be due to the difference in SST and SAT used in respective studies. Jaswal et al. (2012) reported that variations in annual mean SST and SAT are not entirely consistent over some local oceanic regions (such as the Bay of Bengal) due to a less thermal adjustment between the upper layers of ocean and lowest atmosphere there.

In terms of seasonal forecasting experience, the persistence of decadal SST variability can offer some degree of decadal predictability. Generally speaking, a long persistence is favorable for a high predictability. Therefore, we further examine the spatial distribution of the persistence of the 5-year mean SST time series, with the aim of testing the robustness of the SST predictability results shown

above. We can see that autocorrelations in the tropical Pacific drop below the 95 % significance level at a lag time of only 5 years, while there are significant autocorrelations up to a lag of 10 years in the North Atlantic, Southern Ocean, North Pacific, and Indo-western Pacific (Fig. 4). Autocorrelations of the 5-year mean SST averaged over the Indo-western Pacific ( $15^{\circ}\text{S}$ – $25^{\circ}\text{N}$ ,  $40^{\circ}$ – $140^{\circ}\text{E}$ ), North Atlantic ( $20^{\circ}$ – $65^{\circ}\text{N}$ ,  $90^{\circ}$ – $0^{\circ}\text{W}$ ), North Pacific ( $20^{\circ}$ – $60^{\circ}\text{N}$ ,  $120^{\circ}\text{E}$ – $120^{\circ}\text{W}$ ), Southern Ocean ( $65^{\circ}$ – $40^{\circ}\text{S}$ ,  $0^{\circ}$ – $360^{\circ}\text{E}$ ), and tropical Pacific ( $5^{\circ}\text{S}$ – $5^{\circ}\text{N}$ ,  $180^{\circ}$ – $85^{\circ}\text{W}$ ) show similar results (Fig. 5). These persistence results suggest that the Indo-western Pacific tends to be more predictable than the tropical Pacific for decadal SST variability, and this is consistent with the predictability results shown above. This consistency adds robustness to the results obtained in the present study.

Figure 6a shows the spatial distribution of the predictability limit of the 9-year low-pass filtered SLP field. We

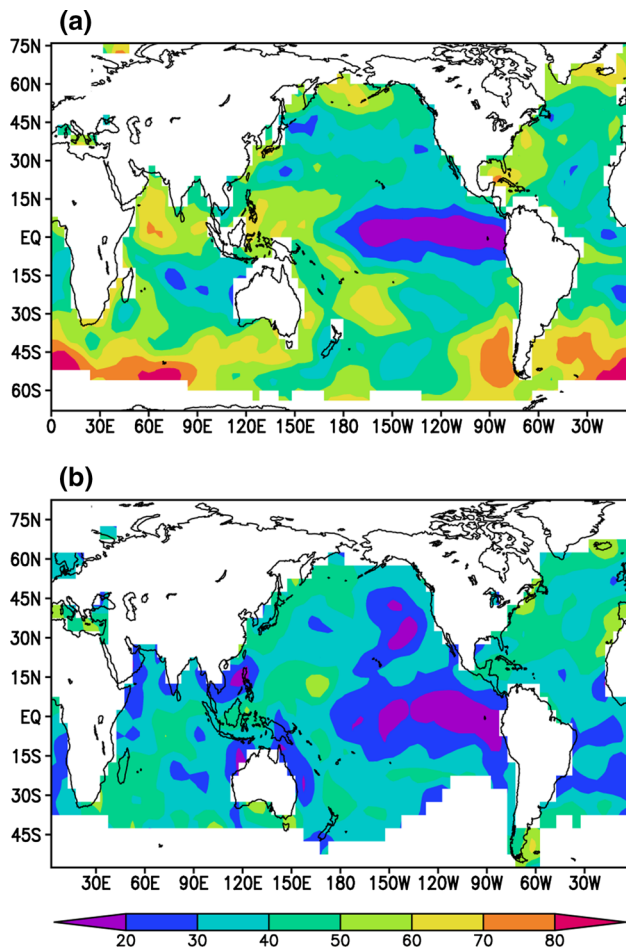


**Fig. 3** **a** The 9-year low-pass filtered variance as a percentage of the total variance of the annual mean SST time series based on the ERSST dataset. **b** As (a), but based on the Kaplan SST dataset

can see that the distributions of the predictability limit of the 9-year low-pass filtered SLP and SST fields are not entirely consistent. There is a relatively large limit of decadal predictability of the SLP over the Antarctic, North Pacific, tropical Indian Ocean, and subtropical North Atlantic (>6 years), which is similar to the situation for SST. However, the predictability limit of the 9-year low-pass filtered SLP field is relatively low (4–7 years) in the North Atlantic poleward of 20°N, and this differs to the SST field. In addition, note that a high decadal predictability for SLP also occurs over the land regions of Africa, India, and South America. Boer (2000) reported that over interannual and longer timescales, there may be some predictability over certain land areas induced by that over the oceans. Autocorrelations of the 5-year mean SLP time series (Fig. 7) show a relatively long persistence over the Antarctic, North Pacific, subtropical North Atlantic, and some land regions of Africa, India, and South America, which generally closely follows the distribution of the predictability limit in Fig. 6a.

Similar to the SST field, the predictability limit of decadal SLP variability was also found to be related to its intensity over most global regions (Fig. 6b). The regions where the decadal SLP variability is strong tend to have a large predictability limit, and vice versa. However, it should be noted that some regions, such as the central–eastern equatorial Pacific, show a relatively strong decadal SLP variability, but these regions have a small predictability limit and a relatively short persistence. The reasons responsible for this inconsistency in these regions remain unexplained. We speculate that unlike most other regions (such as the Antarctic and North Pacific) where the high decadal SLP variability is closely related to fluctuations in slowly varying boundary forcing from the underlying SST, the relatively strong decadal SLP variability over the central–eastern equatorial Pacific is less related to the underlying SST (see Fig. 8), thereby possibly causing a relatively low predictability in this region (as discussed below). It indicates that the relationship between decadal SLP variability and predictability may be different for different regions, presumably depending on the sources of decadal SLP variability there; further research is necessary in this regard.

The above results focus on investigating the spatial distributions of the limit of decadal predictability of the SST and SLP fields. As observational data contain the components of both oceanic or atmospheric internal dynamics and external forcings, and it is difficult to separate these components using the NLE method, little is known of the physical processes responsible for spatial differences in SST and SLP predictability. However, we can still gain some knowledge on the related physical processes from the distributions of the limit of decadal predictability of the SST and SLP fields. For example, there is no consensus on the physical mechanisms that are responsible for atmospheric circulation variability over decadal timescales (Liu 2012). There is evidence that much of decadal atmospheric circulation variability arises from internal atmospheric processes (Hasselmann 1976; Yeh and Kirtman 2004, 2006). On the other hand, it has long been recognized that decadal atmospheric circulation variability is related to fluctuations in slowly varying boundary conditions, such as SST, sea ice, soil moisture, and snow cover at the surface (Watanabe and Nitta 1999; Bojariu and Gimeno 2003; Yang et al. 2007; Yuan and Yonekura 2011). If a large part of the decadal atmospheric circulation variability arises from internal atmospheric processes, it is reasonable to speculate that the predictability is limited to some degree by inherently unpredictable chaotic fluctuations in the atmosphere, and therefore has a relatively low limit on decadal timescales. According to our results (described above), decadal SST variability has a high predictability limit, but decadal SLP variability shows low predictability

**Fig. 4** Spatial distributions of the **a** 5-year, **b** 10-year, **c** 15-year, and **d** 20-year lag auto-correlations of the 5-year mean SST time series based on the ERSST dataset. In **a–d**, areas with correlations significant at the 95 % level are shaded

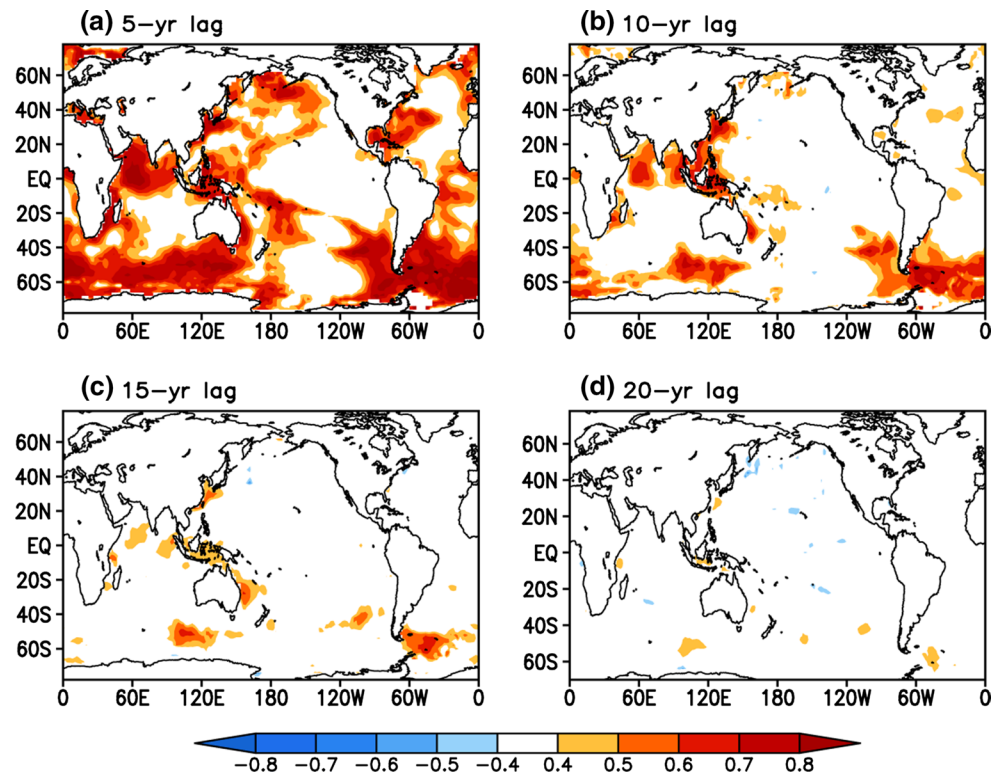
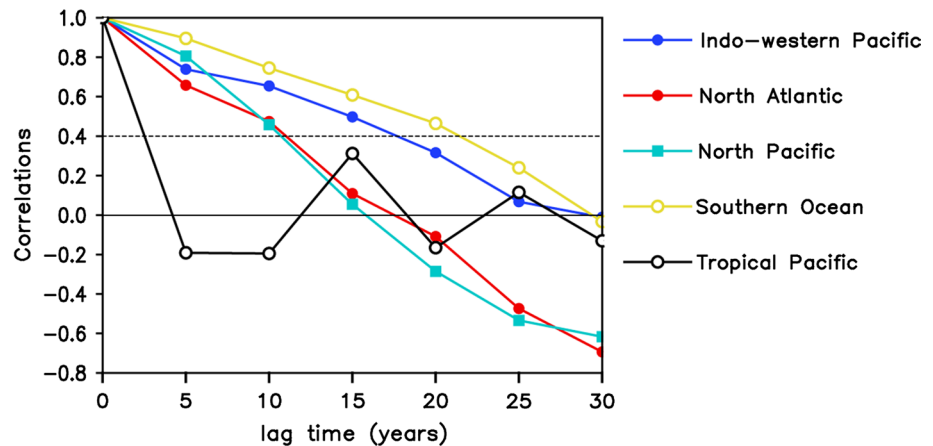


**Fig. 5** Autocorrelations of the 5-year mean SST averaged over the Indo-western Pacific (15°S–25°N, 40°–140°E), North Atlantic (20°–65°N, 90°–0°W), North Pacific (20°–60°N, 120°E–120°W), Southern Ocean (65°–40°S, 0°–360°E), and tropical Pacific (5°S–5°N, 180°–85°W) as a function of lag time. The horizontal dashed line indicates the 95 % significance level



in the North Atlantic poleward of 20°N, possibly indicating that decadal SLP variability there is largely governed by internal atmospheric processes and is less related to the underlying SST. In contrast, there exists a large limit of decadal predictability for both SST and SLP in the North Pacific and high latitudes of the Southern Hemisphere, possibly indicating close coupling between SST and SLP there on decadal timescales.

By examining the correlations of the 5-year mean SST time series with the 5-year mean SLP time series over the oceans (Fig. 8), we find that significant correlation regions are mainly located in the North Pacific, subtropical central eastern North Pacific, subtropical North Atlantic, and high

latitudes of the Southern Hemisphere, generally consistent with a relatively high SLP predictability in these regions. In contrast, there are only weak correlations in the equatorial Pacific and most regions of the North Atlantic poleward of 20°N, which also corresponds well with a relatively low SLP predictability there. These results support our interpretation of the distribution of the limit of decadal predictability of the SLP field.

In other land regions, including Africa, India, and South America, we speculate that decadal variability in the atmospheric circulation might also be associated with decadal variability in the underlying boundary conditions, which may lead to the relatively high limit of decadal



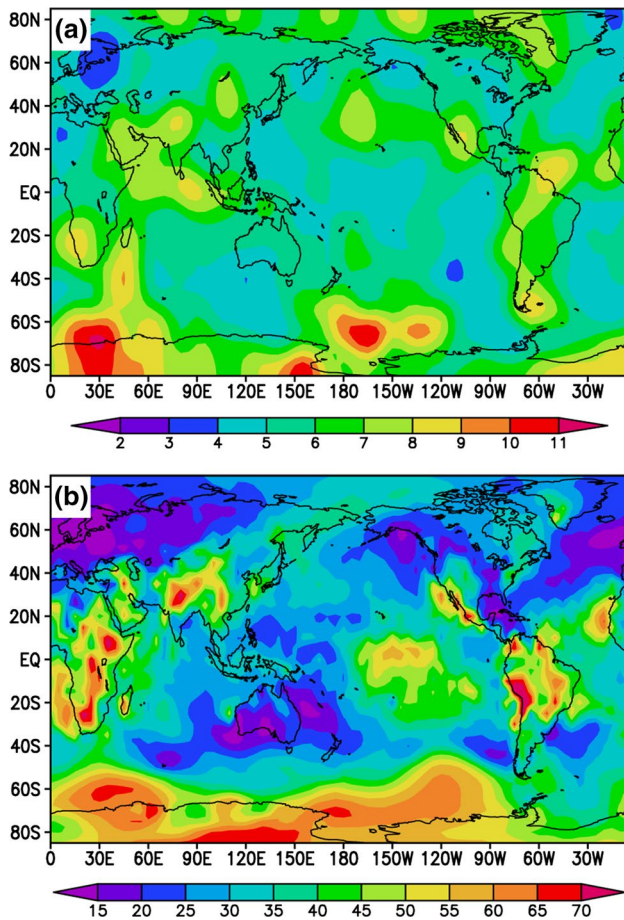


**Fig. 6** **a** Spatial distribution of the predictability limit ( $T_p$ , in years) of the 9-year low-pass filtered SLP based on the HadSLP dataset. **b** Percentage of the 9-year low-pass filtered variance to total variance of the annual mean SLP time series

predictability in SLP. Further study is required to verify this speculation and to provide a detailed understanding of the influence of the interactions between the atmosphere, ocean, and land surface on decadal predictability of variability in the atmospheric circulation.

## 5 Decadal predictability of major climate modes

As the NLE method allows us to determine the predictability limit of decadal SST and SLP variability over a small local region, or for a single grid point, from observational time series, it also enables an estimate of the decadal predictability of major climate modes based on their respective indices. In this section, we will attempt to estimate the limit of decadal predictability of several major climate modes, including the PDO, AMO, NAM, and SAM.

Figure 9a and b shows the mean error growth of the 9-year low-pass filtered PDO and AMO indices, as obtained

using the NLE method. The mean errors of both the PDO and AMO initially increase quickly over about 5 years. Subsequently, the growth of errors slows down and finally reaches saturation. Ding et al. (2010, 2011) reported that this phenomenon of different phases of error growth also occurs in the case of the ISO. They suggested that the initial conditions may play an important role in determining the rapid growth of the mean error of the ISO in the early phase; after about 2 weeks, when the initial conditions have no remaining impact on the error growth, the error growth of the ISO appears to be more strongly influenced by complex nonlinear interactions between the ISO and external forcings (e.g., the slowly varying boundary conditions including SST, soil moisture, etc.). If this also applies to the error growth of the PDO and AMO, as shown above, then we can conclude that the initial conditions related to the PDO and AMO may provide their predictability for 5 years or so, after which natural internal and external forcings for decadal variability (e.g., changes in the thermohaline circulation, solar variability, volcano activity, and aerosol concentrations) can extend their predictability to a longer lead time. This so-called initial-value predictability limit of about 5 years for decadal climate predictions is slightly less than that (of about 7 years) obtained by Branstator and Teng (2010) based on the Community Climate System Model, version 3 (CCSM3) ensemble experiments.

The mean errors of both the PDO and AMO eventually reach saturation (Fig. 9a, b), at which point the prediction becomes meaningless. If the predictability limit is defined as the time at which the error reaches 95 % of its saturation level, the predictability limits of the 9-year low-pass filtered indices of the PDO and AMO are 9 and 11 years, respectively. This result indicates that the predictability limit of the AMO is higher than that of the PDO. From autocorrelations of the 5-year mean PDO and AMO indices (not shown), the persistence of the AMO is also longer than that of the PDO. These results indicate that the AMO tends to be more predictable than the PDO, and this is consistent with the results of previous observational and modeling studies (Kim et al. 2012; van Oldenborgh et al. 2012). Liu (2012) pointed out that, unlike the Pacific, where decadal variability occurs largely in the upper-ocean wind-driven circulation, much of the decadal variability in the Atlantic is often thought to be largely due to an active Atlantic meridional overturning circulation (AMOC). Msadek et al. (2010) reported that the AMOC tends to be a highly predictable component of the ocean state, and may be predictable for up to 20 years. Considering that the AMOC plays an important role in driving the AMO decadal SST variations, the highly predictable AMOC may also bring some predictability to the AMO.

The preceding analysis suggests that the PDO and AMO are predictable out to 10 years or longer, which has

**Fig. 7** As Fig. 4, but for spatial distributions of the **a** 5-year, **b** 10-year, **c** 15-year, and **d** 20-year lag autocorrelations of the 5-year mean SLP time series based on the HadSLP dataset

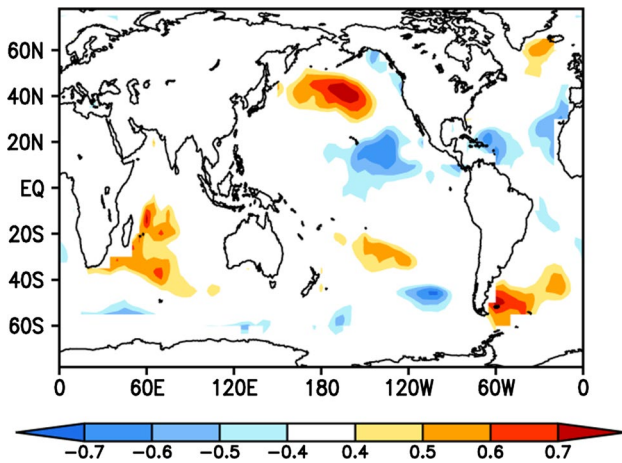
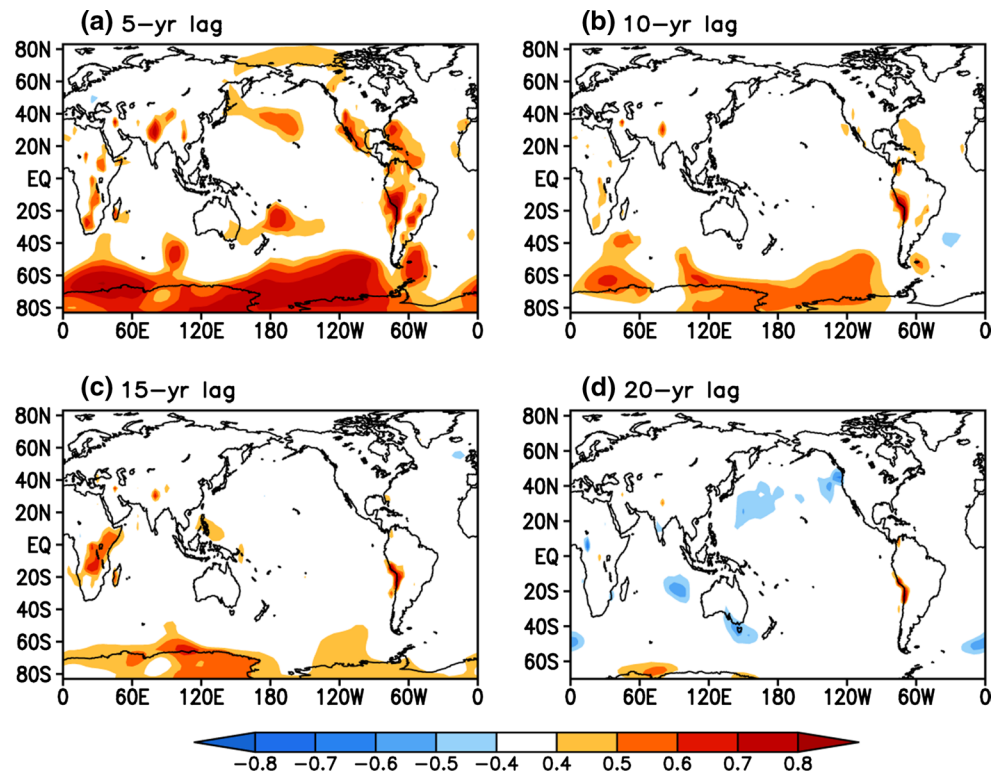


**Fig. 8** Correlations between the 5-year mean SST time series based on the ERSST dataset and the 5-year mean SLP time series based on the HadSLP dataset over the oceans. Areas with correlations significant at the 95 % level are shaded

implications for decadal predictions of surface temperatures and precipitation across North America and Eurasia. Whether major modes of atmospheric variability, such as the NAM and SAM, show similar decadal predictability remains an open question. Numerous studies have examined the predictability of the annular modes; however, most of these studies focus on the impact of slowly evolving boundary conditions (e.g., changes in the stratospheric flow,

mid-high latitude sea ice and SST anomalies, and ENSO) on the amplitude of the NAM or the SAM (e.g., Zhou and Yu 2004; Mukougawa et al. 2009; Lim et al. 2013). The predictability limit of the NAM and SAM over decadal timescales is less clear. Figure 10a and b shows the mean error growth of the 9-year low-pass filtered NAM and SAM indices, respectively. The error growth of the SAM displays two distinct phases: a first fast-growth phase followed by a slow-growth phase, similar to the behavior of the PDO and AMO. In contrast, the error of the NAM grows very rapidly and reaches saturation within a few years. For the NAM, the fast-growth phase of the errors is evident, but the slow-growth phase is absent. We determined the predictability limits of the 9-year low-pass filtered NAM and SAM indices to be around 4 and 9 years, respectively. This result indicates that the predictability limit of the SAM is much higher than that of the NAM, and is comparable with the limit of the PDO obtained above. The relatively higher decadal predictability for the SAM, and the relatively lower decadal predictability for the NAM, are consistent with the distribution of the predictability limit of the 9-year low-pass filtered SLP field (Fig. 6a), which shows that decadal SLP variability has a higher predictability limit over the Antarctic, but has a relatively low predictability limit over the Arctic. As discussed in Sect. 4, it is very likely that decadal predictability of the NAM mainly arises from internal atmospheric processes, while the coupling between the SAM and subpolar SST contributes largely to the predictability of the SAM.

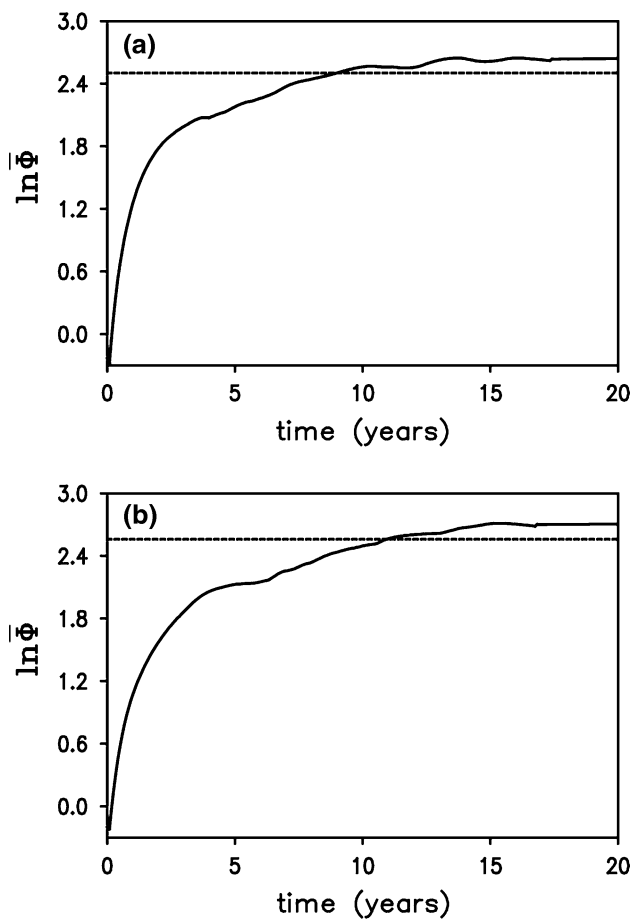


**Fig. 9** Mean error growth of the 9-year low-pass filtered **a** PDO and **b** AMO indices, obtained using the NLLE method. The *dashed line* represents the 95 % level of the saturation value obtained by taking the average of the mean error growth after 15 years

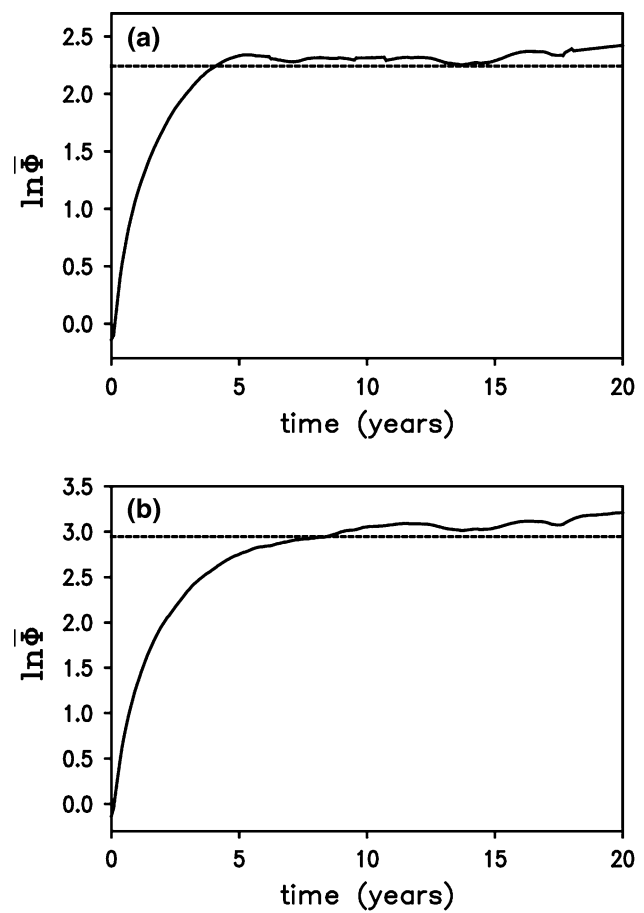


**Fig. 10** As Fig. 9, but for mean error growth of the 9-year low-pass filtered **a** NAM and **b** SAM indices

## 6 Data requirements and predictability due to filtering

The NLLE method estimates the atmospheric and oceanic predictability by searching for the LDA from the observational time series. However, Boer (2000) noted that the analog approach tends to suffer from a lack of sufficiently close initial states in both the real and modeled systems. Lorenz (1969) reported that a sufficiently long time series is required when using historical analogs to study atmospheric predictability, and it is almost impossible to find good natural analogs within current libraries of historical atmospheric data over large regions such as the Northern Hemisphere. However, it should be noted that the LDA is searched for from the observational time series for a small local region or a single grid point, for which the small number of spatial degrees of freedom makes it possible to find good local analogs within current libraries of historical atmospheric or oceanic data

that allow an ensemble average (Ding et al. 2011; Li and Ding 2011).

The time series of the SST and SLP fields at one grid point used in the present study includes about  $12 \times 156 = 1872$  data points. To examine whether this number of data points is sufficient to find good local analogs for decadal variability, we examined the dependence of the estimated decadal predictability limit on the number of data points using a longer record of the reconstructed monthly SLP field from 1659 to 1999 over the eastern North Atlantic and Europe (Luterbacher et al. 2002). The number of data points available for the analogs of the reconstructed SLP was  $12 \times 341 = 4092$ . Figure 11 shows the estimated predictability limit of the 9-year low-pass filtered reconstructed SLP at the grid point  $40^\circ\text{N}$ ,  $160^\circ\text{W}$  as a function of the number of data points. The limit shows a gradual decrease with decreasing number of data points when the number of data points is greater than  $12 \times 101$ . In contrast, when the number of data points is less than  $12 \times 101$ , the limit shows a rapid decrease with decreasing number of data points. This result might be expected,

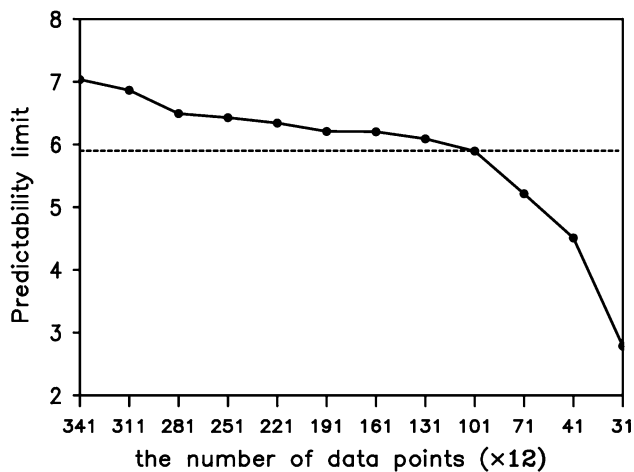


**Fig. 11** Estimated predictability limit of the 9-year low-pass filtered reconstructed SLP at the grid point 30°N, 10°E as a function of the number of data points. *Dashed line* represents the predictability limit obtained using  $101 \times 12$  data points

considering that the initial error will become larger (because good local analogs would be more difficult to be found) for a smaller number of data points (not shown). It is very likely that the initial error shows a rapid increase with a gradual decrease in the number of data points when the number of data points is less than  $12 \times 101$ . The estimated predictability limit decreases by approximately 12 % when using 1872 data points compared with the limit obtained using 4092 data points. Similar results were obtained at other grid points. These results demonstrate that although the approximately 1872 data points used in the present study tend to underestimate the predictability limit to some extent, such an underestimation is relatively slight, indicating that this number of data points is just sufficient to find good local analogs for decadal variability. Consequently, the predictability limits of decadal SST and SLP variability, as obtained in the present study, are meaningful.

We will now consider another important question concerning the influence of temporal filtering on the estimation of decadal predictability. Following on from the above analysis, we applied a 9-year low-pass filter to isolate the decadal signals of the SST and SLP fields and then estimated their predictability using the NLLE method. It should be noted that the use of temporal filtering tends to inflate the estimation of decadal predictability, mainly because the filtered value for the present year contains information from both past and future years. As the filtered value contains future information, it tends to enhance the forecast skill as a result of the propagation of observed information into the forecast data (Seo et al. 2009). Moreover, those predictability limits estimated based on the 9-year low-pass filtered SST and SLP fields are difficult to attain in real time because the temporal filtering has only

limited use in real-time predictions due to its requirement for information beyond the end of the time series (Wheeler and Hendon 2004).

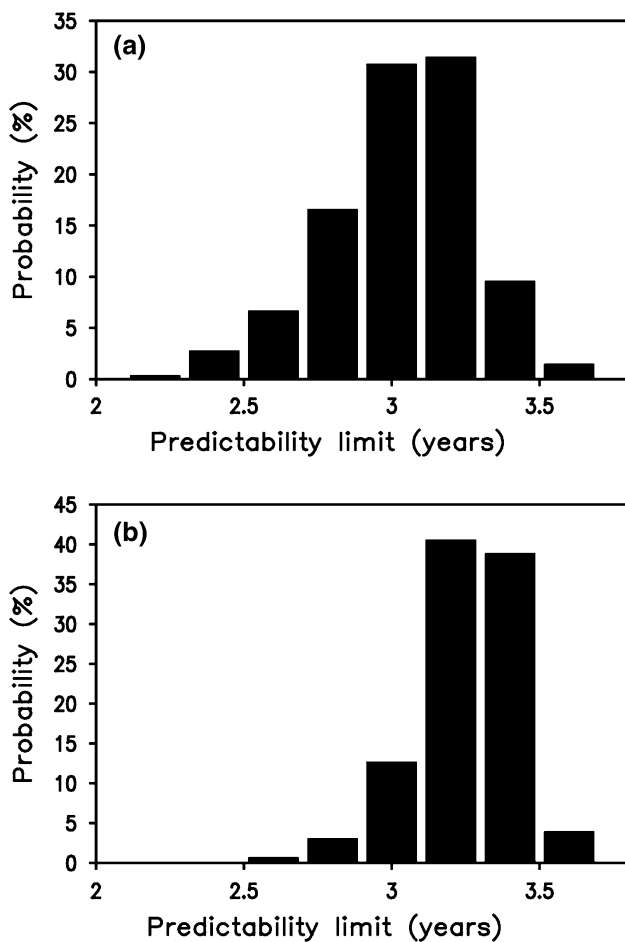
Following Ding et al. (2010, 2011), we applied the Monte Carlo method to test how much predictability is derived from the temporal filtering itself. First, we took the discrete Fourier transform (DFT) of the 9-year low-pass filtered PDO and AMO indices, and generated random numbers that give the same power at each wavenumber and frequency as the 9-year low-pass filtered PDO and AMO indices. Then, we computed the discrete inverse Fourier transform over the wavenumber–frequency band of the PDO and AMO to obtain the filtered noise characterized by the same spectrum as the real PDO and AMO. Finally, we applied the NLLE method to a time series from the filtered noise and tested its predictability. The above procedure was repeated 1000 times, yielding 1000 values of the predictability limit of filtered noise with the same spectral characteristics as the PDO and AMO. A brief description of the above algorithm is given in “Appendix 2”.

Figure 12a, b shows the probability distributions of these values of the predictability limit of filtered noise with the same spectral characteristics as the PDO and AMO, respectively. In both cases, the predictability limits of filtered noise with a maximum probability occur when the limit is about 3 years. Accordingly, we conclude that the temporal filtering itself may bring a predictability of about 3 years. This predictability due to the filtering is much less than the 10-year predictability of the PDO and AMO obtained above, indicating that the estimated predictability of the PDO and AMO mainly arises from the real signal of the physical processes responsible for the PDO and AMO decadal variability, although the filtering tends to extend the predictability to some extent. In contrast, if climate modes such as the NAM have a decadal predictability close to, or slightly greater than, the approximate 3-year predictability of background noise caused by the temporal filtering, it is very likely that a large part of the estimated predictability of these climate modes is artificial, and arises mainly from the filtering itself. It seems that these climate modes are less predictable over decadal timescales. Most of these results are also applicable to local regions of the SLP and SST fields.

## 7 Summary and discussion

This study aimed to investigate the limit of decadal predictability using the NLLE method, which can provide a quantitative estimate of atmospheric and oceanic predictability based on observational data. As the limit of decadal predictability varies widely with region, we first examined the spatial distributions of the limit of decadal





**Fig. 12** Probability distribution of the predictability limits based on filtered background noise, which has the same spectral characteristics as the 9-year low-pass filtered **a** PDO and **b** AMO indices

predictability of the 9-year low-pass filtered SST and SLP fields. The limit of decadal predictability of the SST field is relatively large in the North Atlantic, North Pacific, Southern Ocean, and Indo-western Pacific, exceeding 7 years at most locations in these regions. In contrast, the limit of the SST field is relatively small in the tropical central–eastern Pacific (4–6 years). Similar to the SST field, the SLP field has a relatively large limit of decadal predictability over the Antarctic, North Pacific, and tropical Indian Ocean (>6 years). However, the limit of the SLP field is relatively low in the North Atlantic (4–7 years), and this differs from the SST field. In addition, a relatively large limit of decadal predictability of the SLP field also occurs over the land regions of Africa, India, and South America. Distributions of the limit of decadal predictability of both the SST and SLP fields are almost consistent with those of the intensity and persistence of the decadal SST and SLP variability. The regions where the decadal SST (SLP) variability is strong and has

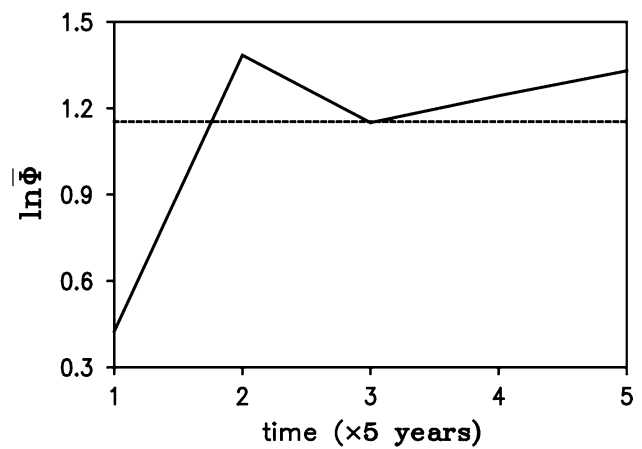


**Fig. 13** Mean error growth of the 5-year mean PDO index, obtained using the NLLE method. The *dashed line* represents the 95 % level of the saturation value obtained by taking the average of the mean error growth after 10 years

a long persistence tend to have a large limit of decadal SST (SLP) predictability, and vice versa.

We used the NLLE method to perform a quantitative analysis of the limit of decadal predictability of several major climate modes, including the PDO, AMO, NAM, and SAM. The limit of decadal predictability of the PDO was found to be about 9 years, which is slightly less than that of the AMO (about 11 years). As the major mode of atmospheric circulation, the SAM has a limit of decadal predictability of about 9 years, which is much higher than that of the NAM (about 4 years). Our investigation of the mean error growth of these climate modes revealed an initial-value predictability limit of about 5 years for decadal prediction.

The above findings lead us to conclude that decadal SST or SLP variability in some regions may be predictable for up to 10 years. This result is encouraging for decadal prediction. However, the use of temporal filtering to extract decadal-scale variability in the present study tends to overestimate the decadal predictability. The limit of decadal predictability based on the time-filtered data, as obtained in the present study, can be regarded as the limit of potential decadal predictability. For real-time decadal prediction, the application of temporal filtering is restricted and the limit of decadal predictability could be lower than the above estimate. Figure 13 shows the mean error growth of the 5-year mean PDO index, which avoids a temporal filtering to extract the decadal signals. The limit of real-time decadal predictability based on this 5-year mean PDO index is higher than 5 years but lower than 10 years, presumably less than the potential predictability obtained from the 9-year low-pass filtered PDO index (about 9 years). Given the relatively short observational records of the PDO index, this comparison between real-time and potential decadal

predictability would inevitably include large uncertainties. Further study is required to assess the differences in real-time and potential decadal predictability by employing the SST and SLP data from a longer period of observations or a long-term simulation of a more realistic model of decadal variability.

Although the limit of decadal predictability may be overestimated in the present study, the spatial variability of the limit of decadal predictability of the SST and SLP fields could be realistic. Decadal prediction could be helped by an improved understanding of the spatial variability of decadal predictability of the SST and SLP fields. As it is difficult for the NLLE method to isolate the individual influence of various physical processes on decadal predictability from the observed SST and SLP data, little is known of the physical processes responsible for spatial differences in the SST and SLP decadal predictability. Further study will be necessary to examine the physical processes that influence local SST and SLP decadal predictability in different regions.

**Acknowledgments** We wish to thank the anonymous reviewers for their constructive comments and suggestions, which helped to substantially improve the quality of this paper. This research was jointly supported by the 973 project of China (2012CB955200), the National Natural Science Foundation of China (41175069), the China Special Fund for Meteorological Research in the Public Interest (GYHY201306031), and the Strategic Priority Research Program of the Chinese Academy of Sciences (XDA11010303).

## Appendix 1: An algorithm for NLLE estimation from observational data

If we obtain the experimental data of a single variable  $x$  of an  $n$ -dimensional chaotic system, or observe the atmospheric or oceanic data of variable  $x$  at one point of  $n$  spatial grid points (e.g., the time series of  $x$  is given by  $\{x(t_i), i = 0, 1, 2, \dots, m - 1\}$  where  $m$  represents the length of the time series), an algorithm that allows an estimation of the mean NLLE from the experimental or observational time series of variable  $x$  is as follows.

Step 1. Taking  $x(t_0)$  as the reference point at time  $t_0$ , we first seek the LDA  $x(t_k)$  of the reference point from the raw series. Two distances (i.e., the initial distance between two points and the evolutionary distance between their trajectories within a short initial period) are used to measure the degree of similarity between the points. All points  $x(t_j)$  ( $|t_j - t_0| > t_D$ ), where  $t_D$  is the time taken for autocorrelations of variable  $x$  to drop to around 0.0, ensuring that a good analog pair is not merely due to persistence) in the raw series form a set  $S$ . The initial distance  $d_i$  between the points  $x(t_0)$  and  $x(t_j)$  is given by

$$d_i = |x(t_0) - x(t_j)|. \quad (8)$$

We assume that the evolutions of the two points are analogous over a very short time  $\tau$ , which is referred to as the initial evolutionary interval, if they are analogous at the initial time. The choice of the initial evolutionary interval  $\tau$  depends on the persistence of variable  $x$ ; if the persistence is low, the time over which two initially close points remain analogous is relatively short. The time taken for autocorrelations of variable  $x$  to drop to 0.9 can be regarded as a rough estimate of the initial evolutionary interval  $\tau$ . A high value (0.9) of autocorrelation is chosen to ensure a short initial evolutionary interval (the results were found to be insensitive to the selected value). Within the initial evolutionary interval  $\tau$  ( $\tau = K\Delta$ ), where  $\Delta$  is the sampling interval of the time series (i.e.,  $\Delta = t_i - t_{i-1}$ ) and  $K$  is the number of sampling intervals over the initial evolutionary interval), the evolutionary distance  $d_e$  between the two points  $x(t_0)$  and  $x(t_j)$  is given by:

$$d_e = \sqrt{\frac{1}{K+1} \sum_{i=0}^K [x(t_i) - x(t_{j+i})]^2}. \quad (9)$$

Here,  $d_i$  is the amount of the initial separation between the two points  $x(t_0)$  and  $x(t_j)$ , while  $d_e$  is the evolutionary distance between their trajectories over the initial evolutionary interval. The total distance  $d_t$ , considering not only the initial distance but also the evolutionary distance, is found by adding  $d_i$  and  $d_e$ :

$$d_t = d_i + d_e. \quad (10)$$

If  $d_t$  is very small, it is highly likely that the points  $x(t_0)$  and  $x(t_j)$  are LDA points at the initial time. Of course, this approach is unlikely to exclude the possibility that only the variable  $x$  and its most relevant variables remain close, whereas other variables evolve very differently over time, especially for high-dimensional dynamical systems. Therefore, the analogs based on variable  $x$  are only local analogs, and they cannot simply be considered as global analogs. The constraint of the total distance  $d_t$ , which contains both initial information and evolutionary information over an initial evolutionary interval, allows us to exclude a large portion of all points with large initial distances, thereby helping us to find a truly local analog for the reference point.

For every point  $x(t_j)$  in the set  $S$ , the value of  $d_t$  can be determined. The nearest neighbor (LDA)  $x(t_k)$  of the reference point  $x(t_0)$  can be chosen from the set  $S$  only if  $d_t$  is the minimum. Then, the initial distance between  $x(t_0)$  and  $x(t_k)$  is denoted as follows:

$$L_1(t_0) = |x(t_0) - x(t_k)|. \quad (11)$$

Step 2. At time  $\tau_i = i \times \Delta$  ( $i = 1, 2, 3, \dots, M$ , where  $M$  is the total number of evolutionary steps),  $x(t_0)$  will have evolved to  $x(t_0 + \tau_i)$  along the reference trajectory, and  $s(t_k)$

will have evolved into  $x(t_k + \tau_i)$  along the analogous trajectory. The initial difference  $L_1(\tau_0)$  will have become:

$$L_1(\tau_i) = |x(t_0 + \tau_i) - x(t_k + \tau_i)|. \tag{12}$$

The growth rate of the initial error during the evolutionary interval  $(\tau_i)$  is:

$$\xi_1(\tau_i) = \frac{1}{\tau_i} \ln \frac{L_1(\tau_i)}{L_1(0)}, \quad (i = 1, 2, 3, \dots, M) \tag{13}$$

With  $i$  gradually increasing, we can obtain the variation of  $\xi_1(\tau_i)$  as a function of the evolution time  $\tau_i$  ( $i = 1, 2, 3, \dots, M$ ).

Step 3. Taking  $x(t_1)$  as the reference state and evolution time  $\tau_i = i \times \Delta$  ( $i = 1, 2, 3, \dots, M$ ), and repeating Steps 1 and 2 above, we obtain the error growth rate  $\xi_2(\tau_i)$  as a function of the evolution time  $\tau_i$ :

$$\xi_2(\tau_i) = \frac{1}{\tau_i} \ln \frac{L_2(\tau_i)}{L_2(0)},$$

where  $L_2 = (0)$  is the initial distance between the reference point  $x(t_1)$  and its LDA, and  $L_2 = (\tau_i)$  is the evolution of  $L_2 = (0)$  with time  $\tau_i$ .

Step 4. The above procedure is repeated until the trajectory reaches the last reference point  $x(t_{m-M-1})$ , and we have error growth rates at all reference points  $\{x(t_0), x(t_1), \dots, x(t_{m-M-1})\}$  given by:

$$\xi_k(\tau_i) = \frac{1}{\tau_i} \ln \frac{L_k(\tau_i)}{L_k(0)}, \quad (k = 1, \dots, N; i = 1, 2, 3, \dots, M)$$

where  $N = m - M$  is the total number of reference points on the reference trajectory,  $\tau_i = i \times \Delta$  ( $i = 1, 2, 3, \dots, M$ ) is the evolution time,  $L_k(0)$  is the initial distance between the reference point  $x(t_k)$  and its LDA, and  $L_k(\tau_i)$  is the evolution of  $L_k(0)$  with the time  $\tau_i$ . It follows that the average of error growth rates at all reference points is:  $\bar{\xi}(\tau_i) = \frac{1}{N} \sum_{k=1}^N \xi_k(\tau_i) = \frac{1}{N} \sum_{k=1}^N \left[ \frac{1}{\tau_i} \ln \frac{L_k(\tau_i)}{L_k(0)} \right] = \frac{1}{\tau_i}$

$\ln \left[ \sqrt[N]{\frac{L_1(\tau_i)}{L_1(0)} \frac{L_2(\tau_i)}{L_2(0)} \dots \frac{L_N(\tau_i)}{L_N(0)}} \right]$ . That is:

$$\exp [\bar{\xi}(\tau_i)\tau_i] = \sqrt[N]{\frac{L_1(\tau_i)}{L_1(0)} \frac{L_2(\tau_i)}{L_2(0)} \dots \frac{L_N(\tau_i)}{L_N(0)}}. \tag{14}$$

Step 5. Observing that the right-hand-side of Eq. (14) is the geometric mean of the relative growth of initial error (RGIE) of all reference points, we obtained the approximation of the mean RGIE:

$$\bar{\Phi}(\tau_i) = \exp [\bar{\xi}(\tau_i)\tau_i], \quad (i = 1, 2, 3, \dots, M). \tag{15}$$

By investigating the evolution of  $\bar{\Phi}(\tau_i)$  with increasing  $\tau_i$ , we can estimate the mean predictability limit of the variable  $x$ .

### Appendix 2: A Monte Carlo algorithm allowing for the estimation of the predictability caused by the temporal filtering itself

Given the time series  $x_n$  ( $n = 1, 2, \dots, N$ ), it was passed through a temporally low-pass filter. The low-pass filtered time series is denoted as  $s_n$  ( $n = 1, 2, \dots, N$ ). An algorithm obtained by applying the Monte Carlo method to test how much predictability is derived from the temporal filtering itself is as follows.

Step 1. For the time series  $s_n$  ( $n = 1, 2, \dots, N$ ), if  $N$  is even, the Fourier series coefficients can be obtained using a discrete Fourier transform (DFT):

$$c_1 = \sum_{n=1}^N s_n$$

$$c_{2m-1} = - \sum_{n=1}^N s_n \sin \left[ \frac{(m-1)(n-1)2\pi}{N} \right], \quad (m = 2, \dots, N/2)$$

$$c_{2m-2} = \sum_{n=1}^N s_n \cos \left[ \frac{(m-1)(n-1)2\pi}{N} \right], \quad (m = 2, \dots, N/2 + 1)$$

If  $N$  is odd,  $c_m$  is defined as above for  $m$  from 2 to  $(N + 1)/2$ .

Step 2. Based on the Fourier series coefficients obtained above, one forms the vector  $P$  of length  $(N + 1)/2$  as follows:

$$P_1 = |c_1|$$

$$P_k = \sqrt{c_{2k-2}^2 + c_{2k-1}^2}, \quad (k = 2, 3, \dots, (N + 1)/2),$$

where  $P_k$  corresponds to the power level at the dominant frequencies of  $s_n$ . Then, we generate random sequence  $R_k$  ( $k = 1, 2, \dots, (N + 1)/2$ ) that gives the same power at each wavenumber and frequency as  $s_n$ .

Step 3. We compute the discrete inverse Fourier transform of  $R_k$  to return the filtered noise sequence  $s'_n$  ( $n = 1, 2, \dots, N$ ) characterized by the same spectrum as  $s_n$ . Specifically, if  $M = (N + 1)/2$  is even, the filtered noise sequence  $s'$  of length  $N$  can be obtained using the discrete inverse Fourier transform of  $R_k$ :

$$s'_n = R_1 + (-1)^{(n-1)}R_M + 2 \sum_{m=2}^{M/2} R_{2m-2} \cos \frac{[(m-1)(n-1)2\pi]}{M} - 2 \sum_{m=2}^{M/2} R_{2m-1} \sin \frac{[(m-1)(n-1)2\pi]}{M}, \quad (n = 1, \dots, N)$$

If  $M$  is odd:

$$s'_n = R_1 + 2 \sum_{m=2}^{(M+1)/2} R_{2m-2} \cos \frac{[(m-1)(n-1)2\pi]}{M} - 2 \sum_{m=2}^{(M+1)/2} R_{2m-1} \sin \frac{[(m-1)(n-1)2\pi]}{M}, \quad (n = 1, \dots, N)$$

Step 4. We apply the NLE method to the filtered noise sequence  $s'_n$  ( $n = 1, 2, \dots, N$ ) and determine its predictability limit.

Step 5. The above procedure is repeated 1000 times, yielding 1000 values of the predictability limit of filtered noise with the same spectral characteristics as  $s_n$ . By analyzing the probability distributions of these values of the predictability limit, we can estimate how much predictability is derived from the temporal filtering itself.

## References

- Allan R, Ansell T (2006) A new globally complete monthly historical gridded mean sea level pressure dataset (HadSLP2): 1850–2004. *J Clim* 19:5816–5842
- Boer GJ (2000) A study of atmosphere–ocean predictability on long time scales. *Clim Dyn* 16:469–472
- Boer GJ (2004) Long time-scale potential predictability in an ensemble of coupled climate models. *Clim Dyn* 23:29–44
- Boer GJ (2011) Decadal potential predictability of twenty-first century climate. *Clim Dyn* 36:1119–1133
- Bojariu R, Gimeno L (2003) The role of snow cover fluctuations in multiannual NAO persistence. *Geophys Res Lett* 30:1156. doi:10.1029/2002GL015651
- Branstator G, Teng H (2010) Two limits of initial-value decadal predictability in a CGCM. *J Clim* 23:6292–6311
- Buermann W, Lintner B, Bonfils C (2005) A wintertime Arctic Oscillation signature on early-season Indian Ocean monsoon intensity. *J Clim* 18:2247–2269
- Chang P, Saravanan R, Ji L (2003) Tropical Atlantic seasonal predictability: the roles of El Niño remote influence and thermodynamic air–sea feedback. *Geophys Res Lett* 30:1501. doi:10.1029/2002GL016119
- Chen BH, Li JP, Ding RQ (2006) Nonlinear local Lyapunov exponent and atmospheric predictability research. *Sci Chin* 49D:1111–1120
- Codron F (2005) Relation between annular modes and the mean state: Southern Hemisphere Summer. *J Clim* 18:320–330
- Collins M (2002) Climate predictability on interannual to decadal time scales: the initial value problem. *Clim Dyn* 19:671–692
- Collins M, Sinha B (2003) Predictability of decadal variations in the thermohaline circulation and climate. *Geophys Res Lett* 30:1306. doi:10.1029/2002GL016504
- Collins M, Frame D, Sinha B, Wilson C (2002) How far ahead could we predict El Niño? *Geophys Res Lett* 29:1492. doi:10.1029/2001GL013919
- Delworth TL, Mann ME (2000) Observed and simulated multidecadal variability in the Northern Hemisphere. *Clim Dyn* 16:661–676
- Deser C, Timlin M (1997) Atmosphere–ocean interaction on weekly timescales in the North Atlantic and Pacific. *J Clim* 10:393–408
- Ding RQ, Li JP (2007) Nonlinear finite-time Lyapunov exponent and predictability. *Phys Lett A* 364:396–400
- Ding RQ, Li JP, Ha KJ (2008) Trends and interdecadal changes of weather predictability during 1950s–1990s. *J Geophys Res* 113:D24112. doi:10.1029/2008JD010404
- Ding RQ, Li JP, Seo KH (2010) Predictability of the Madden–Julian oscillation estimated using observational data. *Mon Weather Rev* 138:1004–1013
- Ding RQ, Li JP, Seo KH (2011) Estimate of the predictability of boreal summer and winter intraseasonal oscillations from observations. *Mon Weather Rev* 139:2421–2438
- Eckmann JP, Ruelle D (1985) Ergodic theory of chaos and strange attractors. *Rev Mod Phys* 57:617–656
- Flato G, Marotzke J, Abiodun B, Braconnot P, Chou SC, Collins W, Cox P, Driouech F, Emori S, Eyring V, Forest C, Gleckler P, Guilyardi E, Jakob C, Kattsov V, Reason C, Rummukainen M (2013) Evaluation of climate models. In: Stocker TF, Qin D, Plattner G-K, Tignor M, Allen SK, Boschung J, Nauels A, Xia Y, Bex V, Midgley PM (eds) *Climate change 2013: the physical science basis. Contribution of Working Group I to the Fifth Assessment Report of the Intergovernmental Panel on Climate Change*. Cambridge University Press, Cambridge, United Kingdom and New York, NY, USA, pp 741–866
- Gong DY, Wang SW (1999) Definition of Antarctic oscillation index. *Geophys Res Lett* 26:459–462. doi:10.1029/1999GL900003
- Goswami BN, Shukla J (1991) Predictability of the coupled ocean–atmosphere model. *J Clim* 4:3–22
- Griffies SM, Bryan K (1997) A predictability study of simulated North Atlantic multidecadal variability. *Clim Dyn* 13:459–488
- Han WQ, Vialard J, McPhaden MJ, Lee T, Masumoto Y, Feng M, de Ruijter WPM (2014) Indian Ocean decadal variability: a review. *Bull Am Meteorol Soc*. doi:10.1175/BAMS-D-13-00028.1
- Hasselmann K (1976) Stochastic climate models. Part I: theory. *Tellus* 28:473–485
- Hurrell JW, Kushnir Y, Visbeck M (2001) The North Atlantic Oscillation. *Science* 291:603–605
- Jaswal AK, Singh V, Bhambak SR (2012) Relationship between sea surface temperature and surface air temperature over Arabian Sea, Bay of Bengal and Indian Ocean. *J Ind Geophys Union* 16:41–53
- Jin EK, Kinter JL, Wang B, Park CK, Kang IS, Kirtman BP, Kug JS, Kumar A, Luo JJ, Schemm J, Shukla J, Yamagata T (2008) Current status of ENSO prediction skill in coupled ocean–atmosphere models. *Clim Dyn* 31:647–664
- Kaplan A, Cane M, Kushnir Y, Clement A, Blumenthal M, Rajagopalan B (1998) Analyses of global sea surface temperature 1856–1991. *J Geophys Res* 103:18567–18589. doi:10.1029/97JC01736
- Kazantsev E (1999) Local Lyapunov exponents of the quasi–geostrophic ocean dynamics. *Appl Math Comput* 104:217–257
- Keenlyside NS, Latif M, Jungclaus J, Kornblueh L, Roeckner E (2008) Advancing decadal-scale climate prediction in the North Atlantic sector. *Nature* 453:84–88
- Kim HM, Webster PJ, Curry JA (2012) Evaluation of short-term climate change prediction in multi-model CMIP5 decadal hindcasts. *Geophys Res Lett* 39:L10701. doi:10.1029/2012GL051644
- Kirtman BP, Schopf PS (1998) Decadal variability in ENSO predictability and prediction. *J Clim* 11:2804–2822
- Knight JR, Folland CK, Scaife AA (2006) Climate impacts of the Atlantic Multidecadal Oscillation. *Geophys Res Lett* 33:L17706. doi:10.1029/2006GL026242
- Kumar A, Chen MY, Wang WQ (2013) Understanding prediction skill of seasonal mean precipitation over the tropics. *J Clim* 26:5674–5681
- Lacarra JF, Talagrand O (1988) Short-range evolution of small perturbations in a barotropic model. *Tellus* 40A:81–95
- Latif M, Anderson D, Barnett T, Cane M, Kleeman R, Leetmaa A, O'Brien J, Rosati A, Schneider E (1998) A review of



- the predictability and prediction of ENSO. *J Geophys Res* 103:14375–14394
- Latif M, Roeckner E, Botzet M, Esch M, Haak H, Hagemann S, Jungclaus JH, Legutke S, Marsland SJ, Mikolajewicz U, Mitchell J (2004) Reconstructing, monitoring, and predicting multidecadal-scale changes in the North Atlantic thermohaline circulation with sea surface temperature. *J Clim* 17:1605–1614
- Latif M, Collins M, Pohlmann H, Keenlyside N (2006) A review of predictability studies of Atlantic sector climate on decadal time scales. *J Clim* 19:5971–5987
- Lau NC, Nath MJ (1996) The role of the atmospheric bridge in linking tropical Pacific ENSO events to extratropical SST anomalies. *J Clim* 9:2036–2057
- Li JP, Ding RQ (2008) Temporal-spatial distributions of predictability limit of short-term climate. *Chin J Atmos Sci* 32:975–986 (in Chinese with English abstract)
- Li JP, Ding RQ (2011) Temporal-spatial distribution of atmospheric predictability limit by local dynamical analogues. *Mon Weather Rev* 139:3265–3283
- Li JP, Ding RQ (2013) Temporal-spatial distribution of the predictability limit of monthly sea surface temperature in the global oceans. *Int J Climatol* 33:1936–1947
- Li JP, Wang JXL (2003) A modified zonal index and its physical sense. *Geophys Res Lett* 30:1632. doi:10.1029/2003GL017441
- Li JP, Wang S (2008) Some mathematical and numerical issues in geophysical fluid dynamics and climate dynamics. *Commun Comput Phys* 3:759–793
- Lienert F, Doblas-Reyes FJ (2013) Decadal prediction of interannual tropical and North Pacific sea surface temperature. *J Geophys Res Atmos* 118:5913–5922. doi:10.1002/jgrd.50469
- Lim EP, Hendon HH, Rashid H (2013) Seasonal predictability of the southern annular mode due to its association with ENSO. *J Clim* 26:8037–8054
- Liu ZY (2012) Dynamics of interdecadal climate variability: a historical perspective. *J Clim* 25:1963–1995
- Liu XH, Ding RQ (2007) The relationship between the spring Asian atmospheric circulation and the previous winter Northern Hemisphere annular mode. *Theor Appl Climatol* 88:71–81
- Lorenz EN (1963) Deterministic nonperiodic flow. *J Atmos Sci* 20:130–141
- Lorenz EN (1965) A study of the predictability of a 28-variable atmospheric model. *Tellus* 17:321–333
- Lorenz EN (1969) Atmospheric predictability as revealed by naturally occurring analogues. *J Atmos Sci* 26:636–646
- Luterbacher J, Xoplaki E, Dietrich D, Rickli R, Jacobeit J, Beck C, Gyalistras D, Schmutz C, Wanner H (2002) Reconstruction of sea level pressure fields over the Eastern North Atlantic and Europe back to 1500. *Clim Dyn* 18:545–561
- Mantua NJ, Hare SR (2002) The Pacific decadal oscillation. *J Oceanogr* 58:35–44
- Mantua NJ, Hare SR, Zhang Y, Wallace JM, Francis RC (1997) A Pacific interdecadal climate oscillation with impacts on salmon production. *Bull Am Meteorol Soc* 78:1069–1079
- Marshall J, Kushner Y, Battisti D, Chang P, Czaja A, Dickson R, Hurrell J, McCartney M, Saravanan R, Visbeck M (2001) North Atlantic climate variability: phenomena, impacts, and mechanisms. *Int J Climatol* 21:1863–1898
- Meehl GA, Goddard L, Murphy JM, Stouffer RJ, Boer G, Danabasoglu G, Dixon KW, Giorgetta MA, Greene AM, Hawkins E (2009) Decadal prediction: can it be skillful? *Bull Am Met Soc* 90:1467–1485
- Mehta V, Meehl G, Goddard L, Knight J, Kumar A, Latif M, Lee T, Rosati A, Stammer D (2011) Decadal climate predictability and prediction: where are we? *Bull Am Meteorol Soc* 92:637–640
- Molinari RL, Mestas-Nuñez AM (2003) North Atlantic decadal variability and the formation of tropical storms and hurricanes. *Geophys Res Lett* 30:1541. doi:10.1029/2002GL016462
- Msadek R, Dixon KW, Delworth TL, Hurlin W (2010) Assessing the predictability of the Atlantic meridional overturning circulation and associated fingerprints. *Geophys Res Lett* 37:L19608. doi:10.1029/2010GL044517
- Mu M (2000) Nonlinear singular vectors and nonlinear singular values. *Sci Chin* 43D:375–385
- Mukougawa H, Hirooka T, Kuroda Y (2009) Influence of stratospheric circulation on the predictability of the tropospheric Northern Annular Mode. *Geophys Res Lett* 36:L08814. doi:10.1029/2008GL037127
- Murphy J, Kattsov V, Keenlyside N, Kimoto M, Meehl G, Mehta V, Pohlmann H, Scaife A, Smith D (2010) Towards prediction of decadal climate variability and change. *Procedia Environ Sci* 1:287–304
- Nan SL, Li JP (2003) The relationship between summer precipitation in the Yangtze River valley and the boreal spring Southern Hemisphere annular mode. *Geophys Res Lett* 30:2266. doi:10.1029/2003GL018381
- Nidheesh A, Lengaigne M, Vialard J, Unnikrishnan A, Dayan H (2012) Decadal and long-term sea level variability in the tropical Indo-Pacific Ocean. *Clim Dyn* 41:381
- O’Kane TJ, Mateara RJ, Chamberlain MA, Risbeya JS, Sloyana BM, Horenko I (2013) Decadal variability in an OGCM Southern Ocean: intrinsic modes, forced modes and metastable states. *Ocean Model* 69:1–21
- Ostermeier GM, Wallace JM (2003) Trends in the North Atlantic Oscillation-Northern Hemisphere annular mode during the twentieth century. *J Clim* 16:336–341
- Pohlmann H, Botzet M, Latif M, Roesch A, Wild M, Tschuck P (2004) Estimating the decadal predictability of a coupled AOGCM. *J Clim* 17:4463–4472
- Pohlmann H, Jungclaus JH, Kohl A, Stammer D, Marotzke J (2009) Initializing decadal climate predictions with the GECCO oceanic synthesis: effects on the North Atlantic. *J Clim* 22:3926–3938
- Prieto L, Garcia R, Diaz J, Hernandez E, del Teso T (2002) NAO influence on extreme winter temperatures in Madrid (Spain). *Ann Geophys* 20:2077–2085
- Reynolds RW, Smith TM (1994) Improved global sea surface temperature analysis using optimum interpolation. *J Clim* 7:929–948
- Schlesinger M, Ramankutty N (1994) An oscillation in the global climate system of period 65–70 years. *Nature* 367:723–726
- Seo KH, Wang W, Gottschalck J, Zhang Q, Schemm JKE, Higgins WR, Kumar A (2009) Evaluation of MJO forecast skill from several statistical and dynamical forecast models. *J Clim* 22:2372–2388
- Shukla J (1984) Predictability of time averages, Part II. The influence of the boundary forcing. In: Burridge DN, Kallen E (eds) Problems and prospects in long and medium range weather forecasting. Springer, Berlin, pp 155–206
- Smith TM, Reynolds RW, Peterson TC, Lawrimore J (2008) Improvements to NOAA’s historical merged land-ocean surface temperature analysis (1880–2006). *J Clim* 21:2283–2296
- Stammerjohn SE, Martinson DG, Smoth RC, Yuan XJ, Rind D (2008) Trends in Antarctic annual sea ice retreat and advance and their relation to El Niño-Southern oscillation and southern annular mode variability. *J Geophys Res* 113:C03S90. doi:10.1029/2007JC004269
- Sutton RT, Hodson DLR (2005) Atlantic Ocean forcing of North American and European summer climate. *Science* 309:115–118
- Tang YM, Kleeman R, Moore AM (2005) Reliability of ENSO dynamical predictions. *J Atmos Sci* 62:1770–1791

- Thompson DWJ, Wallace JM (1998) The Arctic oscillation signature in the wintertime geopotential height and temperature fields. *Geophys Res Lett* 25:1297–1300. doi:[10.1029/98GL00950](https://doi.org/10.1029/98GL00950)
- Trenberth KE, Jones PD, Ambenje P, Bojariu R, Easterling D, Tank AK, Parker D, Rahimzadeh F, Renwick JA, Rusticucci M, Soden B, Zhai P (2007) Observations: surface and atmospheric climate change. In: Solomon S, Qin D, Manning M, Chen Z, Marquis M, Averyt KB, Tignor M, Miller HL (eds) *Climate change 2007: the physical science basis*. Contribution of Working Group I to the Fourth Assessment Report of the Intergovernmental Panel on Climate Change. Cambridge University Press, Cambridge, United Kingdom and New York, NY, USA, pp 235–336
- van Oldenborgh GJ, Doblas-Reyes FJ, Wouters B, Hazeleger W (2012) Decadal prediction skill in a multi-model ensemble. *Clim Dyn* 38:1263–1280
- Verdy A, Marshall J, Czaja A (2005) Sea surface temperature variability along the path of the Antarctic circumpolar current. *J Phys Oceanogr* 36:1317–1331
- Wang B et al (2009) Advance and prospectus of seasonal prediction: assessment of APCC/CliPAS 14-model ensemble retrospective seasonal prediction (1980–2004). *Clim Dyn* 33:93–117
- Watanabe M, Nitta T (1999) Decadal changes in the atmospheric circulation and associated surface climate variations in the Northern Hemisphere winter. *J Clim* 12:494–510
- Wheeler M, Hendon HH (2004) An all-season real-time multivariate MJO index: development of an index for monitoring and prediction. *Mon Weather Rev* 132:1917–1932
- Yang XY, Wang DX, Wang J, Huang RX (2007) Connection between the decadal variability in the Southern Ocean circulation and the southern annular mode. *Geophys Res Lett* 34:L16604. doi:[10.1029/2007GL030526](https://doi.org/10.1029/2007GL030526)
- Yeh SW, Kirtman BP (2004) The impact of internal atmospheric variability on the North Pacific SST variability. *Clim Dyn* 22:721–732
- Yeh SW, Kirtman BP (2006) Origin of decadal El Niño–Southern Oscillation-like variability in a coupled general circulation model. *J Geophys Res* 111:C01009. doi:[10.1029/2005JC002985](https://doi.org/10.1029/2005JC002985)
- Yoden S, Nomura M (1993) Finite-time Lyapunov stability analysis and its application to atmospheric predictability. *J Atmos Sci* 50:1531–1543
- Yuan XJ, Yonekura E (2011) Decadal variability in the Southern Hemisphere. *J Geophys Res* 116:D19115. doi:[10.1029/2011JD015673](https://doi.org/10.1029/2011JD015673)
- Zhang Y, Wallace JM, Battisti DS (1997) ENSO-like interdecadal variability. *J Clim* 10:1004–1020
- Zhang R, Delworth TL, Held IM (2007) Can the Atlantic Ocean drive the observed multidecadal variability in Northern Hemisphere mean temperature? *Geophys Res Lett* 34:L02709. doi:[10.1029/2006GL028683](https://doi.org/10.1029/2006GL028683)
- Zheng F, Zhu J, Zhang RH, Zhou GQ (2006) Ensemble hindcasts of SST anomalies in the tropical Pacific using an intermediate coupled model. *Geophys Res Lett* 33:L19604. doi:[10.1029/2006GL026994](https://doi.org/10.1029/2006GL026994)
- Zhou TJ, Yu RC (2004) Sea-surface temperature induced variability of the southern annular mode in an atmospheric general circulation model. *Geophys Res Lett* 31:L24206. doi:[10.1029/2004GL021473](https://doi.org/10.1029/2004GL021473)
- Ziehmann C, Smith LA, Kurths J (2000) Localized Lyapunov exponents and the prediction of predictability. *Phys Lett A* 4:237–251